

Article

Exploring the Nature of Silicon-Noble Gas Bonds in $H_3SiNgNSi$ and $HSiNgNSi$ Compounds (Ng = Xe, Rn)

Sudip Pan, Ranajit Saha and Pratim K. Chattaraj *

Department of Chemistry and Centre for Theoretical Studies, Indian Institute of Technology, Kharagpur 721302, India; E-Mails: sudip.chem88@gmail.com (S.P.); ranajitsahachem@gmail.com (R.S.)

* Author to whom correspondence should be addressed; E-Mail: pkc@chem.iitkgp.ernet.in; Tel.: +91-3222-283-304; Fax: +91-3222-255-303.

Academic Editor: Habil. Mihai V. Putz

Received: 11 February 2015 / Accepted: 16 March 2015 / Published: 19 March 2015

Abstract: *Ab initio* and density functional theory-based computations are performed to investigate the structure and stability of $H_3SiNgNSi$ and $HSiNgNSi$ compounds (Ng = Xe, Rn). They are thermochemically unstable with respect to the dissociation channel producing Ng and H_3SiNSi or $HSiNSi$. However, they are kinetically stable with respect to this dissociation channel having activation free energy barriers of 19.3 and 23.3 kcal/mol for $H_3SiXeNSi$ and $H_3SiRnNSi$, respectively, and 9.2 and 12.8 kcal/mol for $HSiXeNSi$ and $HSiRnNSi$, respectively. The rest of the possible dissociation channels are endergonic in nature at room temperature for Rn analogues. However, one three-body dissociation channel for $H_3SiXeNSi$ and one two-body and one three-body dissociation channels for $HSiXeNSi$ are slightly exergonic in nature at room temperature. They become endergonic at slightly lower temperature. The nature of bonding between Ng and Si/N is analyzed by natural bond order, electron density and energy decomposition analyses. Natural population analysis indicates that they could be best represented as $(H_3SiNg)^+(NSi)^-$ and $(HSiNg)^+(NSi)^-$. Energy decomposition analysis further reveals that the contribution from the orbital term (ΔE_{orb}) is dominant (ca. 67%–75%) towards the total attraction energy associated with the Si-Ng bond, whereas the electrostatic term (ΔE_{elstat}) contributes the maximum (ca. 66%–68%) for the same in the Ng–N bond, implying the covalent nature of the former bond and the ionic nature of the latter.

Keywords: *ab initio* study; dissociation channels; kinetic stability; natural population analysis; electron density analysis; energy decomposition analysis

1. Introduction

Having a late break-through in 1962 with the discovery of $\text{Xe}^+[\text{PtF}_6]^-$, chemistry related to the noble gas (Ng) compounds has been developing very rapidly, especially during the last two decades. This is due to the outcome of the huge efforts made by both experimentalists [1–19] and theoreticians [20–46] towards the syntheses and/or predictions of stable Ng-containing compounds. The first compound having the Xe–C bond was reported as XeCH_3^+ many years ago in 1961 by Field *et al.* [47], and the very next year, the same group [48] detected ArCH_3^+ and KrCH_3^+ in mass spectrum. A few years later in 1979, Turbini *et al.* [49] detected $\text{Xe}(\text{CF}_3)_2$ by means of mass spectroscopic techniques. Subsequently, detection of a few pentafluorophenylxenon cation [50–52] derivatives was also reported in 1989. Thereafter, plenty of examples with Ng–C bonds, *viz.* HXeCCH [53–55], HKrCCH [55], HXeCC [53,55], HXeCCXeH [53,55], HXeCN [5], HKrCN [5], HNgCCF [56], HCCNgF [56], ClXeCN [57], BrXeCN [57], HXeC_3N [58], HKrC_3N [58], HXeC_4H [11] and HKrC_4H [11], were made available in the literature as experimentally-detected compounds using a low temperature matrix-isolation technique. Moreover, several theoretically-predicted compounds with Ng–C bonds, some unusual highly-coordinated $\text{Ng}(\text{CCH})_4$ and $\text{Ng}(\text{CCH})_6$ clusters (Ng = Kr, Xe) [59] and polymer, $\text{H}-(\text{Xe}-\text{C}_2)_n-\text{Xe}-\text{H}$ ($n \geq 1$) [60], were found to be metastable species.

On the other hand, there are only a few examples of the systems having Si–Ng bonds, which were experimentally obtained or theoretically predicted to be viable. The generation of the F_3SiXe^+ by Grandinetti *et al.* [61] in an ion-molecule reaction between the protonated SiF_4 and Xe, $\text{F}_3\text{Si}-\text{FH}^+ + \text{Xe} \rightarrow \text{Xe}-\text{SiF}_3^+ + \text{HF}$, provided the first system with the Si–Ng bond. Through so-called direct addition of SiF_3^+ and Ng, Cunje *et al.* [62] were successful in producing not only XeSiF_3^+ , but also ArSiF_3^+ and KrSiF_3^+ at room temperature and high pressure. Two other isomers of NgSiF_3^+ with Si–Ng–F and F–Ng–F types of linkages were also proposed [62]. The metastability of the first neutral compound, FArSiF_3 , with the Si–Ar chemical bond, was predicted by Cohen *et al.* [63]. Prompted by this study, Yockel *et al.* [64] found viable FKrSiF_3 as the first example having the Si–Kr bond in a neutral system. Lundell and coworkers [65] further assessed the stability and bonding of FXeSiF_3 , the first neutral compound with the Si–Xe covalent bond. Roithová *et al.* [66] showed that SiF_3^{2+} could behave as a superelectrophilic reagent and that NgSiF_2^{2+} (Ng = Ne, Ar) could be formed as a result of the thermal ion-molecule reaction, $\text{F}_3\text{Si}^{2+} + \text{Ng} \rightarrow \text{NgSiF}_2^{2+} + \text{F}$. Recently, Savoca *et al.* [67] detected Si_4Xe^+ via infrared (IR) multiple photon dissociation spectroscopy. More recently, we studied the Ng binding ability of the SiH_3^+ cluster, as well as the effect of H substitution of SiH_3^+ by halide groups (–X) on its ability in binding Ng [68].

In this manuscript, we have reported two new viable compounds, $\text{H}_3\text{SiNgNSi}$ and HSiNgNSi (Ng = Xe, Rn), with Si–Ng covalent bonds. Crabtree and coworkers [69] very recently detected highly stable silicon nitrides, H_3SiNSi and HSiNSi by chirped-pulse Fourier transform microwave (CP-FTMW) spectroscopy. H_3SiNSi has a C_{3v} point group symmetry with a linear Si–N–Si moiety,

whereas HSiNSi possesses a planar geometry (C_s) with a slightly bent Si–N–Si arrangement, and for both of them, the minimum energy structures have a singlet spin state. We have assessed *in silico* the structure, stability and the nature of bonding in $H_3SiNgNSi$ and $HSiNgNSi$ compounds. They are found to be metastable systems. The nature of bonding therein is analyzed by natural population analysis (NPA), Wiberg bond indices (WBI) calculation [70], electron density analysis [71] and energy decomposition analysis (EDA) [72–75]. It may be noted that except for $RnSiX_3^+$ ($X = H, F-Br$) [68], there is no study with the compound having the Si–Rn bond. In that sense, for the first time, we reported here the neutral Rn-containing compounds, $H_3SiRnNSi$ and $HSiRnNSi$, with the Si–Rn covalent bond.

2. Results and Discussion

2.1. Structure and Stability

The optimized geometries of H_3SiNSi and $HSiNSi$ compounds and their Ng inserted analogues, $H_3SiNgNSi$ and $HSiNgNSi$, are provided in Figure 1. Similar to their mother moieties, the minimum energy structure of $H_3SiNgNSi$ corresponds to the C_{3v} point group with the 1A_1 electronic state, whereas $HSiNgNSi$ has a planar geometry with the C_s point group and $^1A'$ electronic state. On the other hand, the transition states (TSs) corresponding to the dissociations of $H_3SiNgNSi$ and $HSiNgNSi$ into Ng and H_3SiNSi or $HSiNSi$ have C_s (TS-1 in Figure 1) and C_1 (TS-2 in Figure 1) symmetry, respectively, in which the NSi fragment remains attached with H_3SiNg or $HSiNg$ fragments in a tilted fashion. The geometrical parameters of $H_3SiNgNSi$ and $HSiNgNSi$ compounds obtained at the $\omega B97X-D/def2-QZVPPD$ and $CCSD(T)/def2-TZVP$ levels are provided in Table S1 (Supplementary Information), whereas the same for the minimum energy and TS structures of $H_3SiNgNSi$ and $HSiNgNSi$ obtained at the $MP2/def2-QZVPPD$ level are given in Table 1. The geometrical parameters of H_3SiNSi and $HSiNSi$ are also provided in Table S2 (Supplementary Information). The Si–Ng bond distance in $H_3SiNgNSi$ is somewhat shorter than that in $HSiNgNSi$. This may be due to the positive charges on the Ng centers in $H_3SiNgNSi$ and $HSiNgNSi$ compounds. The positive charge on the Ng center in $H_3SiNgNSi$ (+0.61 |e| on Xe and +0.68 |e| on Rn) is larger than that in $HSiNgNSi$ (+0.50 |e| on Xe and +0.57 |e| on Rn). The chemical inertness of Ng atoms originates from the filled valence shell. Hence, a more positively-charged Ng center would be more effective in taking part in chemical bond formation. The larger interaction energy between H_3Si and NgNSi than that between HSi and NgNSi corroborates well with the stronger bond formation in the former cases than the latter ones (*vide infra*).

The N–Si bond gets slightly elongated in the Ng inserted analogues compared to those in H_3SiNSi and $HSiNSi$. The Si–Ng–N and Ng–N–Si moieties in the $H_3SiNgNSi$ compound are linear. However, the same in the $HSiNgNSi$ compound are slightly bent from the linear arrangement ($\leq 0.5^\circ$). Since in TS-1 and TS-2, the NSi fragment is bonded to the Ng center in a tilted fashion, having the mode with imaginary frequency as the bending of Si–Ng–N and Ng–N–Si angles, the $\angle Si-Ng-N$ and $\angle Ng-N-Si$ get shortened ($96.0^\circ-126.2^\circ$) compared to those in the corresponding minimum energy structures ($\sim 180.0^\circ$). In the TSs, the Si–Ng bond distance is found to decrease by about 0.1 Å, while the Ng–N bond distance increases by 0.3–0.2 Å compared to those in the corresponding minimum energy structures.

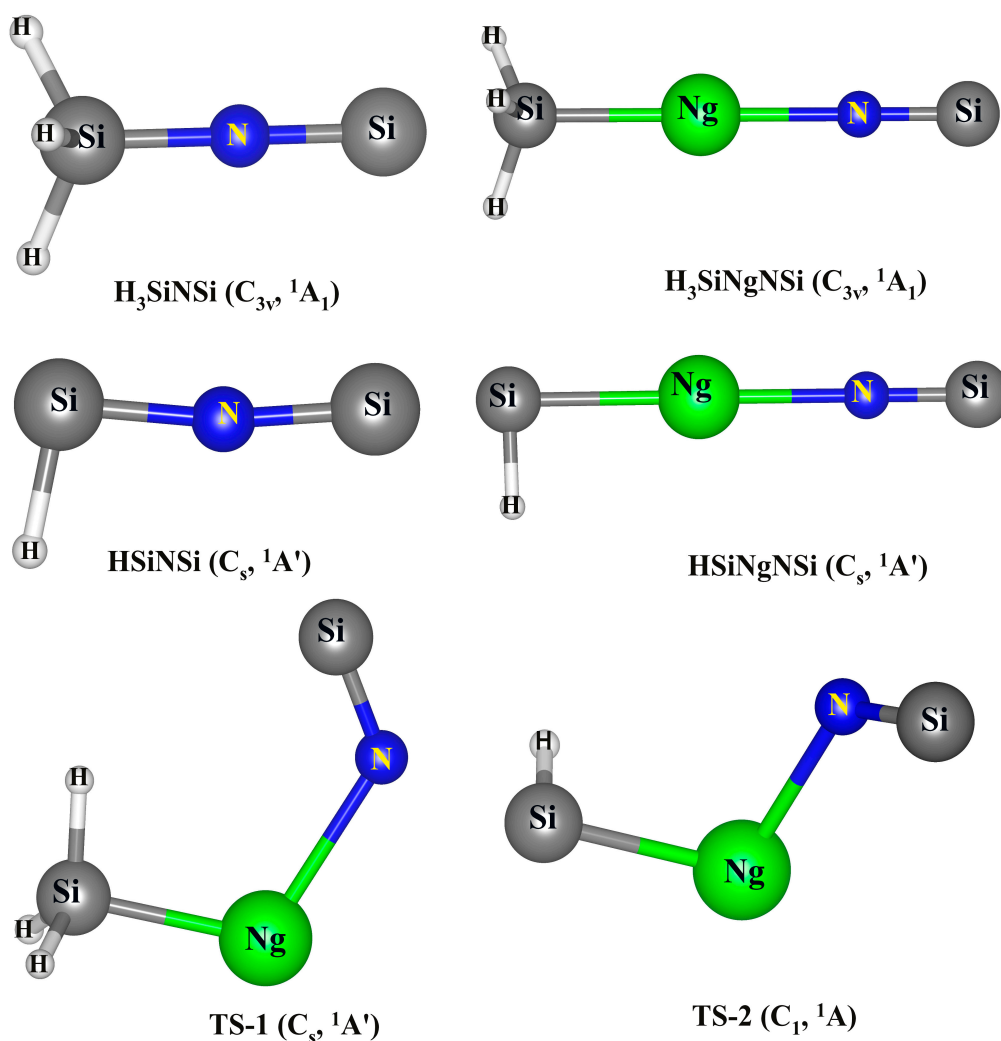


Figure 1. Pictorial depictions of the energy minimum structures and the transition states (TSs) of H_3SiNSi , $HSiNSi$, $H_3SiNgNSi$ and $HSiNgNSi$ compounds. Point groups along with their electronic states are given in parentheses. **TS-1** and **TS-2** are associated with the dissociation of $H_3SiNgNSi$ and $HSiNgNSi$, producing Ng and H_3SiNSi or $HSiNSi$.

Table 1. The geometrical parameters (in Å and degrees) of the optimized geometries of $H_3SiNgNSi$ and $HSiNgNSi$ compounds (both minimum energy structures and transition states) studied at the MP2/def2-QZVPPD level.

Nature of Stationary Points	Compounds	r_{H-Si}	r_{Si-Ng}	r_{Ng-N}	r_{N-Si}	$\angle H-Si-Ng$	$\angle Si-Ng-N$	$\angle Ng-N-Si$
Minimum	$H_3SiXeNSi$	1.471	2.588	2.338	1.600	107.0	180.0	180.0
Energy	$H_3SiRnNSi$	1.472	2.688	2.382	1.598	107.8	180.0	180.0
Structures	$HSiXeNSi$	1.508	2.653	2.375	1.603	88.7	179.5	178.6
	$HSiRnNSi$	1.510	2.747	2.420	1.601	89.0	179.7	179.9
Transition	$H_3SiXeNSi$	1.462(3)	2.486	2.683	1.616	103.9, 99.5	110.6	126.2
States	$H_3SiRnNSi$	1.463(5)	2.573	2.733	1.616	104.1, 99.3	103.7	125.9
	$HSiXeNSi$	1.504	2.511	2.576	1.626	87.6	100.7	125.6
	$HSiRnNSi$	1.505	2.590	2.623	1.625	87.7	96.0	125.5

The stability of these Ng inserted compounds is understood by computing ZPE-corrected dissociation energy (D_0), as well as dissociation enthalpy (ΔH) and free energy change (ΔG) at 298 K for different possible dissociation channels. We have considered the higher spin states of all of the dissociated products. The spin state, which gives the lowest energy, is taken into consideration. We have computed ΔG values for the different possible dissociation channels of $H_3SiNgNSi$ and $HSiNgNSi$ at both the MP2/def2-QZVPPD (see Table S3 in the Supplementary Information) and $\omega B97X-D/def2-QZVPPD$ levels (see Table 2), and those for the D_0 and ΔH are given in Tables S4 and S5 (Supplementary Information). We found that the D_0 , ΔH and ΔG values obtained at the MP2 level are larger than those obtained at the $\omega B97X-D$ level in most cases, particularly in Xe analogues. In some cases, this provides qualitatively wrong results. For example, with respect to most of the dissociation channels, the Xe inserted compounds are less likely to be dissociated than those of the Rn analogues, implying larger stability of the former compounds than the latter ones. However, in general, it is expected that due to larger polarizability, Rn would make a somewhat stronger bond than that of Xe. It was already reported in the literature that the MP2 level of computation can produce inaccurate dissociation energy diagrams for the Ng inserted compounds [76]. Our results corroborate that the stability of Ng inserted compounds should not be analyzed based on MP2 results alone. Therefore, we have given special emphasis to the results obtained at the $\omega B97X-D$ level to assess the stability of these studied compounds with respect to the different dissociation channels.

We have considered two-body (2-B) as well as three-body (3-B) dissociation channels comprising both neutral and ionic fragments. For $H_3SiNgNSi$, except for the 2-B dissociation channel producing H_3SiNSi and Ng, all other dissociation channels are endergonic in nature at room temperature. Though dissociation of $H_3SiNgNSi$ into H_3SiNSi , and Ng is exergonic by -119.3 kcal/mol for Xe and -110.5 kcal/mol for Rn, the dissociation is kinetically protected by 19.3 and 23.3 kcal/mol for Xe and Rn analogues, respectively. For $H_3SiXeNSi$, except this 2-B dissociation, another 3-B dissociation producing H_3Si , Ng and NSi is slightly exergonic in nature (-0.2 kcal/mol) at room temperature. However, it becomes endergonic (2.6 kcal/mol) at a slightly lower temperature (250 K), as the contribution from the favorable ΔS term becomes smaller at a lower temperature.

In the case of $HSiRnNSi$, except for the dissociation into $HSiNSi$ and Rn, all other dissociation channels are endergonic in nature. However, for $HSiXeNSi$, in addition to the dissociation into $HSiNSi$ and Xe, two other 2-B and 3-B dissociations are slightly exergonic in nature at 298 K. In both Xe and Rn analogues, the dissociation producing $HSiNSi$ and Ng is highly exergonic, being -121.1 kcal/mol for Xe and -113.0 kcal/mol for Rn. This dissociation is found to be kinetically protected by the free energy barrier of 9.2 kcal/mol for Xe and 12.8 kcal/mol for Rn analogues. The 2-B dissociation of $HSiXeNSi$ producing $HSiXe$ and NSi and the 3-B dissociation producing HSi, Xe and NSi are exergonic by -3.6 and -5.8 kcal/mol, respectively, at 298 K. We have computed ΔG values at a lower temperature and have found that at 180 K, ΔG values become slightly positive (0.5 and 0.2 kcal/mol for 2-B and 3-B dissociations, respectively), and at 150 K, it becomes 1.6 kcal/mol for the 2-B dissociation and 1.7 kcal/mol for the 3-B dissociation. It may be noted that activation free energy barriers obtained at the MP2 level are quite close to those obtained at the $\omega B97X-D$ level (see Table S3).

Table 2. Free energy change (ΔG , kcal/mol) at 298 K for different dissociation channels of $H_3SiNgNSi$ and $HSiNgNSi$ compounds at the $\omega B97X-D/def2-QZVPPD$ level.

Processes	ΔG		Processes	ΔG	
	Xe	Rn		Xe	Rn
$H_3SiNgNSi \rightarrow H_3SiNg^+ + NSi^-$	105.3	110.7	$HSiNgNSi \rightarrow HSiNg^+ + NSi^-$	99.1	103.8
$H_3SiNgNSi \rightarrow H_3Si^- + NgNSi^+$	165.2	166.1	$HSiNgNSi \rightarrow HSiNg + NSi$	-3.6	3.8
$H_3SiNgNSi \rightarrow H_3SiNSi + Ng$	-119.3	-110.5	$HSiNgNSi \rightarrow HSi^- + NgNSi^+$	163.6	163.9
$H_3SiNgNSi \rightarrow H_3Si + Ng + NSi$	-0.2	8.6	$HSiNgNSi \rightarrow HSiNSi + Ng$	-121.1	-113.0
$H_3SiNgNSi \rightarrow H_3Si^+ + Ng + NSi^-$	122.0	130.8	$HSiNgNSi \rightarrow HSi + Ng + NSi$	-5.8	2.4
$H_3SiNgNSi \rightarrow H_3Si^- + Ng + NSi^+$	201.6	210.4	$HSiNgNSi \rightarrow HSi^+ + Ng + NSi^-$	112.9	121.1
$H_3SiNgNSi \rightarrow H_2Si + NgH + NSi$	64.4	73.0	$HSiNgNSi \rightarrow HSi^- + Ng + NSi^+$	199.9	208.1
$H_3SiNgNSi \rightarrow H_2Si^+ + NgH + NSi^-$	206.6	215.2	$HSiNgNSi \rightarrow Si + NgH + NSi$	87.7	95.7
$H_3SiNgNSi \rightarrow H_2Si^- + NgH + NSi^+$	271.9	280.6	$HSiNgNSi \rightarrow Si + NgH^+ + NSi^-$	220.2	221.9
$H_3SiNgNSi \rightarrow H_2Si + NgH^+ + NSi^-$	196.9	199.2	$\Delta G^{\ddagger a}$	9.2	12.8
$H_3SiNgNSi \rightarrow H_2Si^- + NgH^+ + NSi$	236.9	239.2	–	–	–
$H_3SiNgNSi \rightarrow HSi + HNgH + NSi$	149.4	149.8	–	–	–
$H_3SiNgNSi \rightarrow HSi^+ + HNgH + NSi^-$	268.1	268.4	–	–	–
$H_3SiNgNSi \rightarrow HSi^- + HNgH + NSi^+$	355.1	355.5	–	–	–
$\Delta G^{\ddagger a}$	19.3	23.3	–	–	–

$\Delta G^{\ddagger a}$ is the activation free energy barrier for the processes, $H_3SiNgNSi \rightarrow H_3SiNSi + Ng$ and $HSiNgNSi \rightarrow HSiNSi + Ng$.

Hu and co-workers [77] argued that to have a half-life in the order of $\sim 10^2$ s at 100, 200 and 300 K, a system of type $XNgY$ must have a minimum energy barrier of 6, 13 and 21 kcal/mol, respectively. Therefore, $H_3SiNgNSi$ could be detected at as high as a 250–300 K temperature range, whereas $HSiNgNSi$ could be detected around the 150–200 K temperature range.

2.2. Nature of Bonding

The NPA charge at each atomic center and the WBI values of Si–Ng and Ng–N bonds are tabulated in Table 3. The H and N centers are electronegative in nature, while Si and Ng centers are electropositive in nature. The Si center attached to N (0.77–0.80 $|e|$) carries a slightly more positive charge than that of Si in the $-SiH_3$ fragment (0.51–0.63 $|e|$). On the other hand, N attains a large negative charge of $-1.50 |e|$ for Xe analogues and $-1.52(4) |e|$ for Rn analogues. Note that the net charge on the NSi fragment ranges from $-0.71 |e|$ to $-0.75 |e|$. Therefore, they could be best represented as $(H_3SiNg)^+(NSi)^-$ and $(HSiNg)^+(NSi)^-$. Obviously, the Ng–N bond would be of the ionic type. The low WBI values (~ 0.2) for the Ng–N bonds dictate their ionic nature of interaction. In contrast, the quite high WBI values (~ 0.65) for the Si–Ng bonds imply that the bonds are of the covalent type, and almost a single bond is formed therein.

Table 3. Natural population analysis (NPA) charge on each atomic center (q_k , au) and Wiberg bond indices (WBI) values of Si–Ng and Ng–N bonds computed at the MP2/def2-QZVPPD level.

Compounds	q_k				WBI		
	H	Si	Ng	N	Si–Ng	Ng–N	
H ₃ SiXeNSi	−0.17	+0.63	+0.61	−1.50	+0.79	0.64	0.22
H ₃ SiRnNSi	−0.17	+0.56	+0.68	−1.52	+0.80	0.65	0.22
HSiXeNSi	−0.33	+0.56	+0.50	−1.50	+0.77	0.63	0.18
HSiRnNSi	−0.33	+0.51	+0.57	−1.54	+0.79	0.66	0.17

Electron density analysis [71] provides additional insight into the nature of bonding. Different topological descriptors of electron density and electron localization function (ELF) computed at the bond critical points (BCPs) of Si–Ng and Ng–N bonds are given in Table 4. The concentration and depletion of electron density at the BCPs are indicated by the negative and positive values of $\nabla^2\rho(\mathbf{r}_c)$, respectively. In general, the occurrence of electron density concentration and depletion at the BCPs indicates the covalent and noncovalent type of bonding, respectively. However, many failures ([71,78–83] pp. 312–314) of this descriptor in representing a covalent bond, especially for the systems with heavy atoms, are documented in the literature. The local electron energy density ($H(\mathbf{r}_c)$), which is the sum of local kinetic energy density ($G(\mathbf{r}_c)$) and local potential energy density ($V(\mathbf{r}_c)$), is also commonly applied to interpret the nature of a bond.

Table 4. Calculated topological properties (au) at the bond critical points of Ng–Si and Ng–N bonds obtained from the .wfn files generated at the MP2/def2-QZVPPD level.

Compounds	$\rho(\mathbf{r}_c)$	$\nabla^2\rho(\mathbf{r}_c)$	$G(\mathbf{r}_c)$	$V(\mathbf{r}_c)$	$H(\mathbf{r}_c)$	ELF
H ₃ Si–●–XeNSi	0.078	−0.093	0.016	−0.055	−0.039	0.868
H ₃ SiXe–●–NSi	0.073	0.140	0.057	−0.079	−0.022	0.295
H ₃ Si–●–RnNSi	0.075	−0.061	0.018	−0.051	−0.033	0.824
H ₃ SiRn–●–NSi	0.073	0.139	0.058	−0.081	−0.023	0.284
HSi–●–XeNSi	0.069	−0.056	0.017	−0.049	−0.032	0.786
HSiXe–●–NSi	0.068	0.137	0.053	−0.072	−0.019	0.278
HSi–●–RnNSi	0.066	−0.042	0.017	−0.045	−0.028	0.769
HSiRn–●–NSi	0.068	0.132	0.053	−0.073	−0.020	0.276

Even if $\nabla^2\rho(\mathbf{r}_c) > 0$, but $H(\mathbf{r}_c) < 0$, then also the bond might be considered as a covalent type [84]. In our cases, $\nabla^2\rho(\mathbf{r}_c)$ is negative in the Si–Ng bonds, implying their covalent nature. However, $H(\mathbf{r}_c)$ is negative in both Si–Ng and Ng–N bonds and slightly more negative in Si–Ng bonds than that in Ng–N bonds. The contour plots of $\nabla^2\rho(\mathbf{r})$ are displayed in Figure 2.

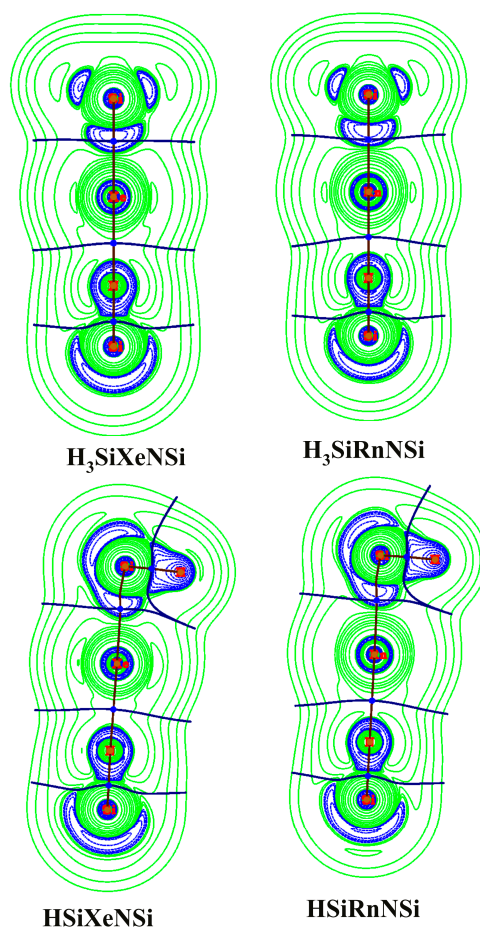


Figure 2. Contour plots of the Laplacian of the electron density of $\text{H}_3\text{SiXeNSi}$ and HSiXeNSi clusters at a particular plane computed at the MP2/def2-QZVPPD/WTBS level (WTBS is used for Xe and Rn; The green-colored region shows the area of $\nabla^2\rho(\mathbf{r}) > 0$, whereas the blue-colored region shows the area of $\nabla^2\rho(\mathbf{r}) < 0$).

In between Si and Ng centers, a well-defined region having $\nabla^2\rho(\mathbf{r}) < 0$ is developed, whereas in between Ng and N centers, the valence orbitals only undergo slight deformation in their shapes. Note that though $H(\mathbf{r}_c)$ is negative in Ng–N bonds, the charge distribution shows that it would be better to consider them as ionic bonds rather than the covalent ones. To prove this, we have further computed ELF [85] at the BCPs of Si–Ng and Ng–N bonds, and the corresponding color-filled maps of ELF are provided in Figure 3. Generally, a high value of ELF at a certain point is an indicator of the localized electrons therein. It further implies the existence of covalent bonds or lone pairs or core electrons.

A typical covalent bond possesses a large ELF value in between two bonded centers, whereas in the case of an ionic bond, the ELF value at the interstitial positions of the two atoms is very low. In our cases, the ELF values at the BCPs of Si–Ng bonds are quite high (~ 0.8) being close to the limiting value of 1.0 for a perfect localization case, whereas they are quite small (~ 0.3) for the Ng–N cases, corroborating well with their ionic nature. The color-filled maps of ELF further dictate the large degree of electron localization in between Si and Ng centers, whereas it is very small in between Ng and N centers (see Figure 3).

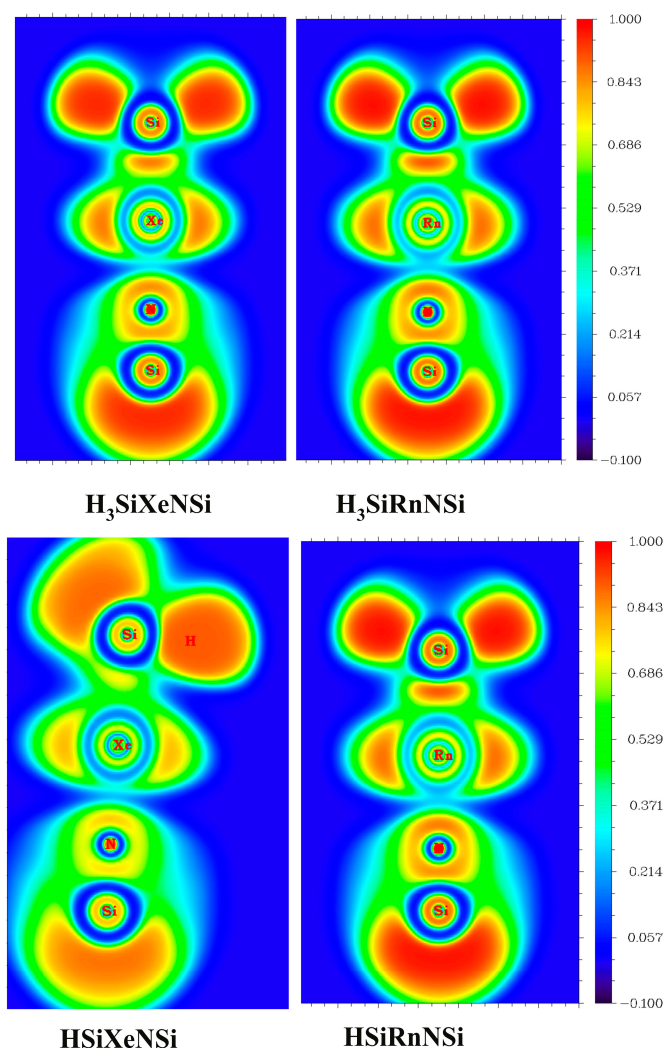


Figure 3. Color-filled maps of the electron localization function of $\text{H}_3\text{SiXeNSi}$ and HSiXeNSi clusters at a particular plane computed at the MP2/def2-QZVPPD/WTBS level (WTBS is used for Xe and Rn).

The total interaction energy (ΔE_{int}) is divided into the Pauli repulsion (ΔE_{pauli}), electrostatic (E_{elstat}), orbital (ΔE_{orb}) and dispersion (ΔE_{disp}) energy terms in EDA to get further insight into the nature of Si–Ng and Ng–N bonds (see Table 5). The NPA charge on each atomic center is used as a guiding tool to impose the charges on the fragments used in our energy partitioning schemes. Since $\text{H}_3\text{SiNgNSi}$ and HSiNgNSi could be best represented as $(\text{H}_3\text{SiNg})^+(\text{NSi})^-$ and $(\text{HSiNg})^+(\text{NSi})^-$, we have used $[\text{H}_3\text{SiNg}]^+$ or $[\text{HSiNg}]^+$ and $[\text{NSi}]^-$ as two fragments to know the nature of the Ng–N bond. As Tonner and Frenking [86] argued, when two different fragmentation schemes are possible, the most favorable one is given by the smallest size of the ΔE_{orb} term. Therefore, we also performed EDA following the radical fragmentation scheme, and indeed, the ionic fragmentation gives a smaller ΔE_{orb} value than that of the radical one. On the other hand, since the total charges on the fragments, $[\text{H}_3\text{Si}]$ or $[\text{HSi}]$ and $[\text{NgNSi}]$, are well below $0.5 |e|$, we have partitioned $\text{H}_3\text{SiNgNSi}$ and HSiNgNSi into neutral $[\text{H}_3\text{Si}]$ or $[\text{HSi}]$ and $[\text{NgNSi}]$ fragments to explore the nature of Si–Ng bond, as the total charges on them are below $0.5 |e|$.

Table 5. Energy decomposition analysis (EDA) results of the H₃SiNgNSi and HSiNgNSi molecules studied at the revPBE-D3/TZ2P//MP2/def2-QZVPPD level. All of the energy terms are in kcal/mol.

Compounds	Fragments	ΔE_{int}	ΔE_{pauli}	ΔE_{elstat}	ΔE_{orb}	ΔE_{disp}
H ₃ SiXeNSi	[H ₃ Si] + [XeNSi]	-46.0	210.4	-82.0 (32.0%)	-172.6 (67.3%)	-1.7 (0.7%)
	[H ₃ SiXe] ⁺ + [NSi] ⁻	-128.1	111.6	-159.4 (66.5%)	-78.6 (32.8%)	-1.7 (0.7%)
H ₃ SiRnNSi	[H ₃ Si] + [RnNSi]	-49.9	198.8	-80.0 (32.2%)	-166.9 (67.1%)	-1.8 (0.7%)
	[H ₃ SiRn] ⁺ + [NSi] ⁻	-132.9	113.0	-166.6 (67.7%)	-77.4 (31.5%)	-1.9 (0.8%)
HSiXeNSi	[HSi] + [XeNSi]	-37.8	169.6	-51.0 (24.6%)	-155.4 (74.9%)	-1.0 (0.5%)
	[HSiXe] ⁺ + [NSi] ⁻	-120.4	103.4	-148.0 (66.2%)	-74.0 (33.1%)	-1.7 (0.8%)
HSiRnNSi	[HSi] + [RnNSi]	-41.0	163.9	-50.9 (24.8%)	-153.0 (74.7%)	-1.1 (0.5%)
	[HSiRn] ⁺ + [NSi] ⁻	-123.7	105.3	-154.4 (67.4%)	-72.7 (31.7%)	-1.9 (0.8%)

(The percentage values within the parentheses show the contribution towards the total attractive interaction $\Delta E_{\text{elstat}} + \Delta E_{\text{orb}} + \Delta E_{\text{disp}}$).

In the Ng–N bonds, the contribution from ΔE_{elstat} towards the total attraction is the maximum ranging within 66%–68%. ΔE_{orb} contributes around 31%–33% towards the total attraction in these bonds. In cases of Si–Ng bonds, ΔE_{orb} is the largest contributor towards the total attraction (*ca.* 67%–75%), implying their covalent nature. In both Ng–N and Si–Ng bonds, ΔE_{disp} is found to be less important, as it contributes the least.

3. Experimental Section

The geometry optimization and the frequency calculation are performed at several levels, *viz.* ω B97X-D/def2-QZVPPD [87,88], MP2/def2-QZVPPD [89] and CCSD(T)/def2-TZVP [90], to ensure that the results obtained are not an artifact of the calculation at a particular level. For the core electrons of Xe and Rn, a quasi-relativistic pseudopotential is used [91]. At both the ω B97X-D/def2-QZVPPD and MP2/def2-QZVPPD levels, H₃SiNgNSi and HSiNgNSi (Ng = Ar–Rn) are found to be minima on the potential energy surface (PES). However, at the CCSD(T)/def2-TZVP level, the calculations for Ar and Kr inserted analogues do not converge; rather, the compounds dissociate into two fragments during optimization. Hence, we exclude those systems from the discussion. The occurrence of only one imaginary frequency with a mode, which leads to the desired products, implies the transition states (TSs) corresponding to the dissociations of H₃SiNgNSi and HSiNgNSi into Ng and H₃SiNSi or HSiNSi. All of these computations are performed by using the Gaussian 09 program package [92]. The atoms-in-molecules (AIM) analysis [71] is carried out by using Multiwfn software [93] at the MP2/def2-QZVPPD/WTBS level. All of electron WTBS [94,95] basis set is used for Xe and Rn.

The energy decomposition analysis (EDA) [72–75] is performed at the revPBE-D3/TZ2P//MP2/def2-QZVPPD [96–98] level using the ADF (2013.01) program package [99]. Scalar relativistic effects are considered for the heavier atoms using the zeroth-order regular approximation (ZORA) [100–102].

4. Conclusions

H₃SiNgNSi and HSiNgNSi (Ng = Xe, Rn) could be considered as metastable compounds. The 2-B dissociation pathways producing Ng and H₃SiNSi or HSiNSi are found to be highly exergonic in

nature at room temperature. However, they are found to be kinetically stable along the same dissociation channel due to their activation free energy barriers of 19.3 and 23.3 kcal/mol for $\text{H}_3\text{SiXeNSi}$ and $\text{H}_3\text{SiRnNSi}$, respectively, and 9.2 and 12.8 kcal/mol for HSiXeNSi and HSiRnNSi , respectively. The Rn analogues have thermochemical stability with respect to all other possible dissociation channels. However, for $\text{H}_3\text{SiXeNSi}$, another 3-B dissociation channel producing H_3Si , Xe and NSi is slightly exergonic in nature at 298 K, but at a slightly low temperature (250 K), it turns out to be endergonic in nature. On the other hand, for HSiXeNSi one 2-B (HSiNg and NSi) and 3-B (HSi , Ng and NSi) dissociation paths are slightly exergonic in nature at room temperature. At low temperature (around 150–180 K), they become endergonic. The rest of the dissociation paths are not feasible. According to the argument of Hu *et al.* [77], $\text{H}_3\text{SiNgNSi}$ could be stable enough to be detected at the 250–300 K temperature range, whereas HSiNgNSi needs a lower temperature (150–200 K) to be detected. The NPA charge suggests that they could be best represented as $(\text{H}_3\text{SiNg})^+(\text{NSi})^-$ and $(\text{HSiNg})^+(\text{NSi})^-$. Consequently, the WBI values for the Ng–N bonds are found to be quite low (~ 0.2), whereas the same for the Ng–Si bonds are quite large (~ 0.65), signifying the covalent nature of the bond. Large ELF values (~ 0.8) and negative values of $\nabla^2\rho(\mathbf{r}_c)$ at the Si–Ng bond critical points further imply its covalent character. As expected from the ionic nature of Ng–N bonds, the maximum contribution in the total attraction energy comes from the ΔE_{elstat} (ca. 66%–68%). On the other hand, ΔE_{orb} is the main contributing term (ca. 67%–75%) in the total attraction energy of Si–Ng bonds, showing their covalent nature.

Supplementary Materials

Supplementary materials can be found at <http://www.mdpi.com/1422-0067/16/03/6402/s1>.

Acknowledgments

Pratim K. Chattaraj would like to thank Department of Science & Technology, New Delhi, for the Jagadish Chandra Bose National Fellowship. Sudip Pan and Ranajit Saha thank Council of Scientific & Industrial Research and University Grants Commission, New Delhi, for their fellowships. We would like to thank Tamal Goswami for his help.

Author Contributions

Sudip Pan performed the computations and wrote the manuscript. Ranajit Saha helped in preparing the manuscript. Pratim K. Chattaraj guided throughout the work, analyzed the results and reviewed the manuscript.

Conflicts of Interest

The authors declare no conflict of interest.

References

1. Bartlett, N. Xenon hexafluoroplatinate (V) $\text{Xe}^+[\text{PtF}_6]^-$. *Proc. Chem. Soc.* **1962**, 218, doi:10.1039/PS9620000197.

2. Pettersson, M.; Lundell, J.; Räsänen, M. Neutral rare-gas containing charge-transfer molecules in solid matrices. II. HXeH, HXeD, and DXeD in Xe. *J. Chem. Phys.* **1995**, *103*, 205.
3. Pettersson, M.; Nieminen, J.; Khriachtchev, L.; Räsänen, M. The mechanism of formation and infrared-induced decomposition of HXeI in solid Xe. *J. Chem. Phys.* **1997**, *107*, 8423.
4. Pettersson, M.; Lundell, J.; Khriachtchev, L.; Isoniemi, E.; Räsänen, M. HXeSH, the first example of a xenon-sulfur bond. *J. Am. Chem. Soc.* **1998**, *120*, 7979–7980.
5. Pettersson, M.; Lundell, J.; Khriachtchev, L.; Räsänen, M. Neutral rare-gas containing charge-transfer molecules in solid matrices. III. HXeCN, HXeNC, and HKrCN in Kr and Xe. *J. Chem. Phys.* **1998**, *109*, 618.
6. Pettersson, M.; Khriachtchev, L.; Lundell, J.; Räsänen, M. A chemical compound formed from water and xenon: HXeOH. *J. Am. Chem. Soc.* **1999**, *121*, 11904–11905.
7. Khriachtchev, L.; Pettersson, M.; Runeberg, N.; Lundell, J.; Räsänen, M. A stable argon compound. *Nature* **2000**, *406*, 874–876.
8. Khriachtchev, L.; Pettersson, M.; Lignell, A.; Räsänen, M. A more stable configuration of HARF in solid argon. *J. Am. Chem. Soc.* **2001**, *123*, 8610–8611.
9. Khriachtchev, L.; Pettersson, M.; Lundell, J.; Tanskanen, H.; Kiviniemi, T.; Runeberg, N.; Räsänen, M. A neutral xenon-containing radical, HXeO. *J. Am. Chem. Soc.* **2003**, *125*, 1454–1455.
10. Khriachtchev, L.; Tanskanen, H.; Cohen, A.; Gerber, R.B.; Lundell, J.; Pettersson, M.; Kiljunen, H.; Räsänen, M. A gate to organokrypton chemistry: HKrCCH. *J. Am. Chem. Soc.* **2003**, *125*, 6876–6877.
11. Tanskanen, H.; Khriachtchev, L.; Lundell, J.; Kiljunen, H.; Räsänen, M. Chemical compounds formed from diacetylene and rare-gas atoms: HKrC₄H and HXeC₄H. *J. Am. Chem. Soc.* **2003**, *125*, 16361–16366.
12. Feldman, V.I.; Sukhov, F.F. Formation and decay of transient xenon dihydride resulting from hydrocarbon radiolysis in a xenon matrix. *Chem. Phys. Lett.* **1996**, *225*, 425–430.
13. Feldman, V.I.; Sukhov, F.F.; Orlov, A.Y. Further evidence for formation of xenon dihydride from neutral hydrogen atoms: A comparison of ESR and IR spectroscopic results. *Chem. Phys. Lett.* **1997**, *280*, 507–512.
14. Thompson, C.A.; Andrews, L. Noble gas complexes with BeO: Infrared spectra of NG–BeO (NG = Ar, Kr, Xe). *J. Am. Chem. Soc.* **1994**, *116*, 423–424.
15. Thompson, C.A.; Andrews, L. Reactions of laser ablated Be atoms with O₂: Infrared spectra of beryllium oxides in solid argon. *J. Chem. Phys.* **1994**, *100*, 8689.
16. Cooke, S.A.; Gerry, M.C.L. XeAuF. *J. Am. Chem. Soc.* **2004**, *126*, 17000–17008.
17. Michaud, M.; Gerry, M.C.L. XeCu covalent bonding in XeCuF and XeCuCl, characterized by fourier transform microwave spectroscopy supported by quantum chemical calculations. *J. Am. Chem. Soc.* **2006**, *128*, 7613–7621.
18. Brock, D.S.; Mercier, H.P.A.; Schrobilgen, G.J. [H(OXeF₂)_n][AsF₆] and [FXe^{II}(OXe^{IV}F₂)_n][AsF₆] (*n* = 1, 2); Examples of xenon(IV) hydroxide fluoride and oxide fluoride cations and the crystal structures of [F₃Xe---FH][Sb₂F₁₁] and [H₅F₄][SbF₆]·2[F₃Xe---FH][Sb₂F₁₁]. *J. Am. Chem. Soc.* **2013**, *135*, 5089–5104.

19. Debackere, J.R.; Mercier, H.P.A.; Schrobilgen, G.J. Noble-gas difluoride complexes of mercury(II): The syntheses and structures of $\text{Hg}(\text{OTeF}_5)_2 \cdot 1.5\text{NgF}_2$ (Ng = Xe, Kr) and $\text{Hg}(\text{OTeF}_5)_2$. *J. Am. Chem. Soc.* **2014**, *136*, 3888–3903.
20. Collins, J.R.; Frenking, G. Are there neutral helium compounds which are stable in their ground state?: A theoretical investigation of HeBCH and HeBeO. *Chem. Phys. Lett.* **1986**, *132*, 330–333.
21. Koch, W.; Frenking, G.; Gauss, J.; Cremer, D.; Collins, J.R. Helium chemistry: Theoretical predictions and experimental challenge. *J. Am. Chem. Soc.* **1987**, *109*, 5917–5934.
22. Frenking, G.; Koch, W.; Gauss, J.; Cremer, D. Stabilities and nature of the attractive interactions in HeBeO, NeBeO, and ArBeO and a comparison with analogs NGLiF, NGBN, and NGLiH (NG = He, Ar). A theoretical investigation. *J. Am. Chem. Soc.* **1988**, *110*, 8007–8016.
23. Koch, W.; Liu, B.; Frenking, G. Theoretical investigations of small multiply charged cations. III. NeN^{2+} . *J. Chem. Phys.* **1990**, *92*, 2464.
24. Frenking, G.; Koch, W.; Reichel, F.; Cremer, D. Light noble gas chemistry: Structures, stabilities, and bonding of helium, neon, and argon compounds. *J. Am. Chem. Soc.* **1990**, *112*, 4240–4256.
25. Jiménez-Halla, C.Ó.; Fernández, I.; Frenking, G. Is it possible to synthesize a neutral noble gas compound containing a Ng–Ng bond? A theoretical study of H–Ng–Ng–F (Ng = Ar, Kr, Xe). *Angew. Chem. Int. Ed.* **2009**, *48*, 366–369.
26. Fernández, I.; Frenking, G. Neutral noble gas compounds exhibiting a Xe–Xe bond: Structure, stability and bonding situation. *Phys. Chem. Chem. Phys.* **2012**, *14*, 14869–14877.
27. Frohn, H.-J.; Bilir, V.; Westphal, U. Two new types of xenon–carbon species: The zwitterion, $1-(\text{Xe}^+)\text{C}_6\text{F}_4^-4-(\text{BF}_3^-)$, and the dication, $[1,4-(\text{Xe})_2\text{C}_6\text{F}_4]^{2+}$. *Inorg. Chem.* **2012**, *51*, 11251–11258.
28. Pan, S.; Contreras, M.; Romero, J.; Reyes, A.; Merino, G.; Chattaraj, P.K. CsLi_7^+ and O_2Li_5^+ as noble gas trapping agents. *Chem. Eur. J.* **2013**, *19*, 2322–2329.
29. Pan, S.; Jalife, S.; Romero, J.; Reyes, A.; Merino, G.; Chattaraj, P.K. Attractive Xe–Li interaction in Li-decorated clusters. *Comput. Theor. Chem.* **2013**, *1021*, 62–69.
30. Pan, S.; Jalife, S.; Kumar, R.M.; Subramanian, V.; Merino, G.; Chattaraj, P.K. Structure and stability of $(\text{NG})_n\text{CN}_3\text{Be}_3^+$ clusters and comparison with $(\text{NG})\text{BeY}^{0/+}$ (NG = Noble Gas and Y = O, S, Se, Te). *ChemPhysChem* **2013**, *14*, 2511–2517.
31. Khatua, M.; Pan, S.; Chattaraj, P.K. Confinement induced binding of noble gas atoms. *J. Chem. Phys.* **2014**, *140*, 164306.
32. Pan, S.; Moreno, D.; Cabellos, J.L.; Romero, J.; Reyes, A.; Merino, G.; Chattaraj, P.K. In quest of strong Be–Ng bonds among the neutral Ng–Be complexes. *J. Phys. Chem. A* **2014**, *118*, 487–494.
33. Pan, S.; Moreno, D.; Cabellos, J.L.; Merino, G.; Chattaraj, P.K. *Ab initio* study on the stability of $\text{Ng}_n\text{Be}_2\text{N}_2$, $\text{Ng}_n\text{Be}_3\text{N}_2$ and NgBeSiN_2 Clusters. *ChemPhysChem* **2014**, *15*, 2618–2625.
34. Pan, S.; Gupta, A.; Mandal, S.; Moreno, D.; Merino, G.; Chattaraj, P.K. Metastable behavior of noble gas inserted tin and lead fluorides. *Phys. Chem. Chem. Phys.* **2015**, *17*, 972–982.
35. Ansbacher, T.; Gerber, R.B. New organic noble molecules: Energetics, stability and potential energy surfaces of HCCXeCCH and HCCrCCH. *Phys. Chem. Chem. Phys.* **2006**, *8*, 4175–4181.
36. Khriachtchev, L.; Räsänen, M.; Gerber, R.B. Noble-gas hydrides: New chemistry at low temperatures. *Acc. Chem. Res.* **2009**, *42*, 183–191.

37. Feldman, V.I.; Kobzarenko, A.V.; Baranova, I.A.; Danchenko, A.V.; Sukhov, F.F.; Tsivion, E.; Gerber, R.B. Direct visualization of the H–Xe bond in xenon hydrides: Xenon isotopic shift in the IR spectra. *J. Chem. Phys.* **2009**, *131*, 151101.
38. Lockyear, J.F.; Douglas, K.; Price, S.D.; Karwowska, M.; Fijałkowski, K.J.; Grochala, W.; Remeš, M.; Roithová, J.; Schröder, D. Generation of the ArCF_2^{2+} dication. *J. Phys. Chem. Lett.* **2010**, *1*, 358–362.
39. Grochala, W. A metastable He–O bond inside a ferroelectric molecular cavity: $(\text{HeO})(\text{LiF})_2$. *Phys. Chem. Chem. Phys.* **2012**, *14*, 14860–14868.
40. Kurzydłowski, D.; Zaleski-Ejgierd, P.; Grochala, W.; Hoffmann, R. Freezing in resonance structures for better packing: XeF_2 becomes $(\text{XeF}^+)(\text{F}^-)$ at large compression. *Inorg. Chem.* **2011**, *50*, 3832–3840.
41. Borocci, S.; Bronzolino, N.; Grandinetti, F. From OBeHe to H_3BOBeHe : Enhancing the stability of a neutral helium compound. *Chem. Phys. Lett.* **2005**, *406*, 179–183.
42. Antoniotti, P.; Bottizzo, E.; Operti, L.; Rabezzana, R.; Borocci, S.; Grandinetti, F. $\text{F}_3\text{Ge-Xe}^+$: A xenon-germanium molecular species. *J. Phys. Chem. Lett.*, **2010**, *1*, 2006–2010.
43. Operti, L.; Rabezzana, R.; Turco, F.; Borocci, S.; Giordani, M.; Grandinetti, F. Xenon–nitrogen chemistry: Gas-phase generation and theoretical investigation of the xenon–difluoronitrenium ion $\text{F}_2\text{N-Xe}^+$. *Chem. Eur. J.* **2011**, *17*, 10682–10689.
44. Jayasekharan, T.; Ghanty, T.K. Prediction of metastable metal-rare gas fluorides: FMRgF ($\text{M} = \text{Be}$ and Mg ; $\text{Rg} = \text{Ar}$, Kr and Xe). *J. Chem. Phys.* **2008**, *128*, 144314.
45. Sirohiwal, A.; Manna, D.; Ghosh, A.; Jayasekharan, T.; Ghanty, T.K. Theoretical prediction of rare gas containing hydride cations: HRgBF^+ ($\text{Rg} = \text{He}$, Ar , Kr , and Xe). *J. Phys. Chem. A* **2013**, *117*, 10772–10782.
46. Manna, D.; Ghosh, A.; Ghanty, T.K. Theoretical prediction of XRgCO^+ ions ($\text{X} = \text{F}$, Cl , and $\text{Rg} = \text{Ar}$, Kr , Xe), *J. Phys. Chem. A* **2013**, *117*, 14282–14292.
47. Field, F.H.; Franklin, J.L. Reactions of gaseous ions. X. Ionic reactions in xenon-methane mixtures. *J. Am. Chem. Soc.* **1961**, *83*, 4509–4515.
48. Field, H.; Head, H.N.; Franklin, J.L. Reactions of gaseous ions. XI. Ionic reactions in krypton-methane and argon-methane mixtures. *J. Am. Chem. Soc.* **1962**, *84*, 1118–1122.
49. Turbini, L.J.; Aikman, R.E.; Lagow, R.J. Evidence for the synthesis of a stable sigma-bonded xenon-carbon compound: Bis(trifluoromethyl)xenon. *J. Am. Chem. Soc.* **1979**, *101*, 5833–5834.
50. Naumann, D.; Tyrre, W.T. The first compound with a stable xenon-carbon bond: ^{19}F - and ^{129}Xe -n.m.r. spectroscopic evidence for pentafluorophenylxenon(II) fluoroborates. *J. Chem. Soc. Chem. Commun.* **1989**, doi:10.1039/C39890000047.
51. Frohn, H.J.; Jacobs, S.; Henkel, G. The Acetonitrile(pentafluorophenyl)xenon(II) cation, $[\text{MeCN-Xe-C}_6\text{F}_5]$: The first structural characterization of a xenon-carbon bond. *Angew. Chem. Int. Ed.* **1989**, *28*, 1506–1507.
52. Frohn, H.J.; Jakobs, S. The pentafluorophenylxenon(II) cation: $[\text{C}_6\text{F}_5\text{Xe}]^+$: The first stable system with a xenon-carbon bond. *J. Chem. Soc. Chem. Commun.* **1989**, doi:10.1039/C39890000625.
53. Khriachtchev, L.; Tanskanen, H.; Lundell, J.; Pettersson, M.; Kiljunen, H.; Räsänen, M. Fluorine-free organoxenon chemistry: HXeCCH , HXeCC , and HXeCCXeH . *J. Am. Chem. Soc.* **2003**, *125*, 4696–4697.

54. Domanskaya, A.; Kobzarenko, A.V.; Tsvion, E.; Khriachtchev, L.; Feldman, V.I.; Gerber, R.B.; Räsänen, M. Matrix-isolation and *ab initio* study of HXeCCH complexed with acetylene. *Chem. Phys. Lett.* **2009**, *481*, 83–87.
55. Tanskanen, H.; Khriachtchev, L.; Lundell, J.; Räsänen, M. Organo-noble-gas hydride compounds HKrCCH, HXeCCH, HXeCC, and HXeCCXeH: Formation mechanisms and effect of ^{13}C isotope substitution on the vibrational properties. *J. Chem. Phys.* **2004**, *121*, 8291.
56. Khriachtchev, L.; Domanskaya, A.; Lundell, J.; Akimov, A.; Räsänen, M.; Misochko, E. Matrix-isolation and *ab initio* study of HNgCCF and HCCNgF molecules (Ng = Ar, Kr, and Xe). *J. Phys. Chem. A* **2010**, *114*, 4181–4187.
57. Arppe, T.; Khriachtchev, L.; Lignell, A.; Domanskaya, A.V.; Räsänen, M. Halogenated xenon cyanides ClXeCN, ClXeNC, and BrXeCN. *Inorg. Chem.* **2012**, *51*, 4398–4402.
58. Khriachtchev, L.; Lignell, A.; Tanskanen, H.; Lundell, J.; Kiljunen, H.; Räsänen, M. Insertion of noble gas atoms into cyanoacetylene: An *ab initio* and matrix isolation study. *J. Phys. Chem. A* **2006**, *110*, 11876–11885.
59. Sheng, L.; Gerber, R.B. High coordination chemically bound compounds of noble gases with hydrocarbons: Ng(CCH)₄ and Ng(CCH)₆, (Ng = Xe or Kr). *J. Chem. Phys.* **2006**, *124*, 231103.
60. Lundell, J.; Cohen, A.; Gerber, R.B. Quantum chemical calculations on novel molecules from xenon insertion into hydrocarbons. *J. Phys. Chem. A* **2002**, *106*, 11950–11955.
61. Cipollini, R.; Grandinetti, F. The gaseous trifluorosilylxenon cation, F₃SiXe⁺: A stable species with a silicon–xenon bond. *J. Chem. Soc. Chem. Commun.* **1995**, doi:10.1039/C39950000773.
62. Cunje, A.; Baranov, V.; Ling, Y.; Hopkinson, A.; Bohme, D.K. Bonding of rare-gas atoms to Si in reactions of rare gases with SiF₃⁺. *J. Phys. Chem. A* **2001**, *105*, 11073–11079.
63. Cohen, A.; Lundell, J.; Gerber, R.B. First compounds with argon-carbon and argon-silicon chemical bonds. *J. Chem. Phys.* **2003**, *119*, 6415.
64. Yockel, S.; Garg, A.; Wilson, A.K. The existence of FKrCF₃, FKrSiF₃, and FKrGeF₃: A theoretical study. *Chem. Phys. Lett.* **2005**, *411*, 91–97.
65. Lundell, J.; Panek, J.; Latajka, Z. Quantum chemical calculations on FXeSiF. *Chem. Phys. Lett.* **2001**, *348*, 147–154.
66. Roithová, J.; Schröder, D. Silicon compounds of neon and argon. *Angew. Chem. Int. Ed.* **2009**, *48*, 8788–8790.
67. Savoca, M.; Langer, J.; Harding, D.J.; Dopfer, O.; Fielicke, A. Incipient chemical bond formation of Xe to a cationic silicon cluster: Vibrational spectroscopy and structure of the Si₄Xe⁺ complex. *Chem. Phys. Lett.* **2013**, *557*, 49–52.
68. Pan, S.; Moreno, D.; Merino, G.; Chattaraj, P.K. Stability of noble-gas-bound SiH₃⁺ clusters. *ChemPhysChem* **2014**, *15*, 3554–3564.
69. Crabtree, K.N.; Martinez, O., Jr.; McCarthy, M.C. Detection of two highly stable silicon nitrides: HSiNSi and H₃SiNSi. *J. Phys. Chem. A* **2013**, *117*, 11282–11288.
70. Wiberg, K.B. Application of the pople-santry-segal CNDO method to the cyclopropylcarbinyll and cyclobutyl cation and to bicyclobutane. *Tetrahedron* **1968**, *24*, 1083–1096.
71. Bader, R.F.W. *Atoms in Molecules: A Quantum Theory*; Clarendon Press: Oxford, UK, 1990.
72. Morokuma, K. Why do molecules interact? The origin of electron donor-acceptor complexes, hydrogen bonding and proton affinity. *Acc. Chem. Res.*, **1977**, *10*, 294–300.

73. Ziegler, T.; Rauk, A. On the calculation of bonding energies by the hartree Fock Slater Method. *Theor. Chim. Acta* **1977**, *46*, 1–10.
74. Ziegler, T.; Rauk, A.; Baerends, E.J. On the calculation of multiplet energies by the Hartree-Fock-Slater Method. *Theor. Chim. Acta* **1977**, *43*, 261–271.
75. Von Hopffgarten, M.; Frenking, G. Energy decomposition analysis. *Wiley Interdiscip. Rev. Comput. Mol. Sci.* **2012**, *2*, 43–62.
76. Lignell, A.; Khriachtchev, L.; Lundell, J.; Tanskanen, H.; Räsänen, M. On theoretical predictions of noble-gas hydrides. *J. Chem. Phys.* **2006**, *125*, 184514.
77. Li, T.-H.; Liu, Y.-L.; Lin, R.-J.; Yeh, T.-Y.; Hu, W.-P. On the stability of noble gas molecules. *Chem. Phys. Lett.* **2007**, *434*, 38–41.
78. Cioslowski, J.; Mixon, S.T. Universality among topological properties of electron density associated with the hydrogen–hydrogen nonbonding interactions. *Can. J. Chem.* **1992**, *70*, 443–449.
79. Cioslowski, J.; Mixon, S.T. Topological properties of electron density in search of steric interactions in molecules: Electronic structure calculations on ortho-substituted biphenyls. *J. Am. Chem. Soc.* **1992**, *114*, 4382–4387.
80. Poater, J.; Visser, R.; Solà, M.; Bickelhaupt, F.M. Polycyclic benzenoids: Why kinked is more stable than straight. *J. Org. Chem.* **2007**, *72*, 1134–1142.
81. Cerpa, E.; Krapp, A.; Vela, A.; Merino, G. The implications of symmetry of the external potential on bond paths. *Chem. Eur. J.* **2008**, *14*, 10232–10234.
82. Macchi, P.; Proserpio, D.M.; Sironi, A.J. Experimental electron density in a transition metal dimer: Metal-metal and metal-ligand Bonds. *J. Am. Chem. Soc.* **1998**, *120*, 13429–13435.
83. Macchi, P.; Garlaschelli, L.; Martinengo, S.; Sironi, A.J. Charge density in transition metal clusters: Supported vs. unsupported metal-metal interactions. *J. Am. Chem. Soc.* **1999**, *121*, 10428–10429.
84. Cremer, D.; Kraka, E. Chemical bonds without bonding electron density—Does the difference electron-density analysis suffice for a description of the chemical bond? *Angew. Chem. Int. Ed.* **1984**, *23*, 627–628.
85. Becke, A.D.; Edgecombe, K.E. A simple measure of electron localization in atomic and molecular systems. *J. Chem. Phys.* **1990**, *92*, 5397.
86. Tonner, R.; Frenking, G. Divalent carbon(0) chemistry, Part 1: Parent compounds. *Chem. Eur. J.* **2008**, *14*, 3260–3272.
87. Chaim J.-D.; Head-Gordon, M. Long-range corrected hybrid density functionals with damped atom-atom dispersion corrections. *Phys. Chem. Chem. Phys.* **2008**, *10*, 6615–6620.
88. Weigend, F.; Ahlrichs, R. Balanced basis sets of split valence, triple zeta valence and quadruple zeta valence quality for H to Rn: Design and assessment of accuracy. *Phys. Chem. Chem. Phys.* **2005**, *7*, 3297–3305.
89. Møller, C.; Plesset, M.S. Note on an approximation treatment for many-electron systems. *Phys. Rev.* **1934**, *46*, 618–622.
90. Pople, J.A.; Head-Gordon, M.; Raghavachari, K. Quadratic configuration interaction. A general technique for determining electro correlation energies. *J. Chem. Phys.* **1987**, *87*, 5968.

91. Peterson, K.A.; Figgen, D.; Goll, E.; Stoll, H.; Dolg, M. Systematically convergent basis sets with relativistic pseudopotentials. II. Small-core pseudopotentials and correlation consistent basis sets for the post-d group 16–18 elements. *J. Chem. Phys.* **2003**, *119*, 11113
92. Frisch, M.J.; Trucks, G.W.; Schlegel, H.B.; Scuseria, G.E.; Robb, M.A.; Cheeseman, J.R.; Scalmani, G.; Barone, V.; Mennucci, B.; Petersson, G.A.; *et al.* *Gaussian 09, Revision C.01*; Gaussian, Inc.: Wallingford, CT, USA, 2010.
93. Lu, T.; Chen, F.W. Multiwfn: A multifunctional wavefunction analyzer. *J. Comput. Chem.* **2012**, *33*, 580–592.
94. Huzinaga, S.; Miguel, B. A comparison of the geometrical sequence formula and the well-tempered formulas for generating GTO basis orbital exponents. *Chem. Phys. Lett.* **1990**, *175*, 289–291.
95. Huzinaga, S.; Klobukowski, M. Well-tempered Gaussian basis sets for the calculation of matrix Hartree–Fock wavefunctions. *Chem. Phys. Lett.* **1993**, *212*, 260–264.
96. Zhang, Y.; Yang, W. Comment on “Generalized Gradient Approximation Made Simple”. *Phys. Rev. Lett.* **1998**, *80*, 890.
97. Grimme, S.; Antony, J.; Ehrlich, S.; Krieg, H. A consistent and accurate *ab initio* parametrization of density functional dispersion correction (DFT-D) for the 94 elements H–Pu. *J. Chem. Phys.* **2010**, *132*, 154104.
98. Van Lenthe, E.; Baerends, E.J. Optimized Slater-type basis sets for the elements 1–118. *J. Comput. Chem.* **2003**, *24*, 1142–1156.
99. Baerends, E.J.; Ziegler, T.; Autschbach, J.; Bashford, D.; Bérces, A.; Bickelhaupt, F.M.; Bo, C.; Boerrigter, P.M.; Cavallo, L.; Chong, D.P.; *et al.* *ADF 2013.01, SCM, Theoretical Chemistry*; Vrije Universiteit: Amsterdam, The Netherlands, 2013.
100. Van Lenthe, E.; Ehlers, A.; Baerends, E.-J. Geometry optimizations in the zero order regular approximation for relativistic effects. *J. Chem. Phys.* **1999**, *110*, 8943.
101. Van Lenthe, E.; Snijders, J.G.; Baerends, E.J. The zero-order regular approximation for relativistic effects: The effect of spin–orbit coupling in closed shell molecules. *J. Chem. Phys.* **1996**, *105*, 650592.
102. Van Lenthe, E.; Baerends, E.J.; Snijders, J.G. Relativistic total energy using regular approximations. *J. Chem. Phys.* **1994**, *101*, 9783.